Final Report

GIT/EES Project A-3210

GEOMETRIC SOFTWARE MODEL DEVELOPMENT

by

M. S. West, J. W. Peifer, D. R. Morehead, J. R. Galt

Contract No. DAAH01-81-D-A003

Prepared for

U.S. ARMY MISSILE COMMAND
Redstone Arsenal, Alabama
DRSMI/RDF

Prepared by

GEORGIA INSTITUTE OF TECHNOLOGY
Engineering Experiment Station
Atlanta, Georgia 30332

September 1982

PREFACE

In March 1982, Georgia Tech began work on a bistatic multipath Doppler computer model for the US Army Missile Command/Radio Frequency Simulation System (MICOM/RFSS) facility in Huntsville, Alabama. This work culminated in June 1982 with the delivery to MICOM of 128 Doppler multipath tables. The receive antenna in all cases was omnidirectional. The primary subject of this report is the Doppler multipath model which was used in the computer implementation. The Beckmann-Barton model was the basis for this implementation and a number of references are available which describe the theory in some detail [1, 2, 3]. The implementation itself was a 6 man-month effort during February, March, and April. David Morehead was primarily responsible for the terrain data bases. James Galt was primarily responsible for the development of the computer scenarios which were run for MICOM. Michael West and John Peifer were responsible for the development of the code which implemented the Beckmann-Barton model. Maurice Long and Steve Zehner acted as technical consultants throughout the program, while Harold Bassett served as Program Manager. The initial software delivery occurred on May 10, 1982 and represented the technical culmination of the project. Subsequent to this delivery, additional data were supplied to RFSS.

TABLE OF CONTENTS

LIST OF FIGURES

SECTION 1

THE BISTATIC MULTIPATH DOPPLER MODEL

1.1 INTRODUCTION

The heart of the geometric software model work is the multipath model. In the area of radar, Barton is an acknowledged authority in multipath modeling and the Georgia Tech computer program is based on two of his papers [1, 2]. Since the implementation is by computer, the integrals presented by Barton were discretized and Doppler shifts were recorded. Multipath modeling work had been done earlier at Georgia Tech on a series of models widely known as TAC ZINGER [4,5]. Since the main interest of TAC ZINGER, however, was speed of computation, a number of numerical shortcuts had been taken which were not appropriate here. In addition, TAC ZINGER does not compute Doppler shifts, and the primary contributions to the multipath are assumed to occur along the line of sight. Consequently, the MICOM/RFSS program was written from scratch while employing many of the concepts embodied in TAC ZINGER.

The multipath model developed for this project separates the multipath signal into diffuse and specular components. This distinction is artificial in that the two cannot be separately measured in the real world. For this application, the diffuse and specular signals are modeled separately because the two components are broadcast independently from two channels on the RFSS array. The assumption is made that the composite of the separately transmitted diffuse and specular signals will adequately represent the actual multipath signal environment.

In addition to signal strength, the frequency distribution of the multipath signal is also of considerable interest. The signal is spread over a range of frequencies due to the relative motion between the missile and target as they fly over the terrain. Simplifying assumptions include (1) assuming there is no spread in frequency caused by motion on the terrain (or vegetation on the terrain), (2) approximating the diffuse spectrum by a histogram based on the Doppler shifts associated with the midpoints of terrain facets, and (3) assuming that the specular signal can be characterized as a line spectrum.

The remainder of this section contains a complete description of the Beckmann-Barton multipath Doppler model as implemented by Georgia Tech. This multipath model resides on several different computers including an SEL CONCEPT 87 and a VAX 11/780. This section also discusses some of the limitations of the model due to the necessary implementation of the results at the RFSS facility, the most stringent requirements being on the RFSS illumination directions and the update rate.

Multipath models require data bases of specific or generic terrain features. The RFSS simulation required two data bases, one for terrain reminiscent of the White Sands Missile Range, and one for the B-70 test range at Eglin Air Force Base. Section 2 discusses the development of these two data bases, the dielectric constants, and other terrain dependent quantities.

The RFSS required accurate multipath data for two different transmitting antennas and a single omni-directional receiving antenna. Thus one of the most important aspects of the analysis was the characterization of the transmitting antenna patterns. The methods and results of this effort are presented in Section 3.

Section 4 primarily discusses matters peculiar to model implementation in the RFSS. These matters include the scenarios which were run and the format of the tables Georgia Tech generated.

1.2 BISTATIC CROSS SECTIONS FOR DIFFUSE MULTIPATH

The diffuse multipath scattering surface is modeled by a rectangular grid of small facets which describe surface height, scattering qualities, and surface tilt. The diffuse multipath model calculates the total diffuse signal by summing the bistatic cross section contributions from each facet in the terrain under consideration. The model assumes that the slopes over the facet are normally distributed with some mean and variance. The bistatic radar cross section, σ , depends on the facet slopes and the variables β and β_o . The variable β_o is defined by the equation

$$\beta_o = \frac{2 \cdot \sigma_h}{d_c} \tag{1}$$

where σ_h is the surface roughness (the RMS surface height) and d_c is the decorrelation distance of surface features (the distance at which one section of terrain is substantially uncorrelated to another section). Neither of these quantities was available in the terrain data furnished by the government. Consequently, β_o was assumed constant at 0.2. This corresponds roughly to one meter height deviations correlated over a distance of ten meters. Both the Eglin and White Sands scenarios used this number.

Barton defines the variable β as the angle between the bisector of the incident and reflected rays at a facet and the facet normal. One can use vector geometry to easily find this quantity as the inverse cosine of the dot product of the normal facet vector with the sum of the incident and reflected normalized vectors.

The acquisition of β is an important step in determining σ . In particular we can now find the factor

$$\sigma^0 = \frac{1}{\tan^2 \beta_o} e^{(-\tan^2 \beta / \tan^2 \beta_o)} \tag{2}$$

which Barton describes as the bistatic radar scattering coefficient [2]. Figure 1 as generated by Torrance and Cook [6], displays the very similar Beckmann coefficient for two values of β_o . It was generated by Torrance and Cook in their paper on models of light reflection [6]. Barton multiplies σ^0 by several

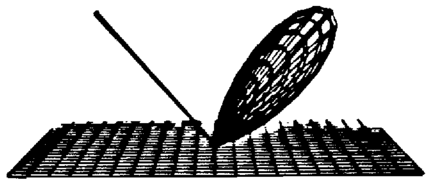

Beckmann distribution for
$\tan\beta_o = 0.2$

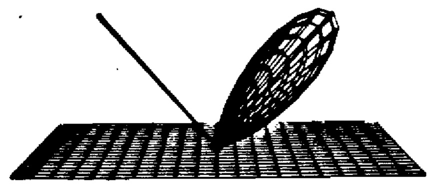

Gaussian distribution for
$\tan\beta_o = 0.2$

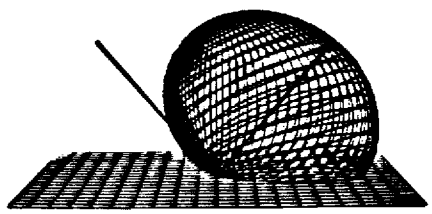

Beckmann distribution for
$\tan\beta_o = 0.6$

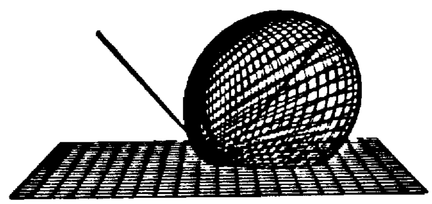

Gaussian distribution for
$\tan\beta_o = 0.6$

Figure 1. Comparison of the Beckmann and Gaussian distributions as calculated in [6].

other terms to obtain the bistatic cross section. In particular, Barton calculates the rms scattering coefficients ρ_{s1} and ρ_{s2} which are functions of the angles ψ_1 and ψ_2. ψ_1 is the angle between the facet and the incident ray and may be calculated by subtracting the inverse cosine of the dot product of the incident vector with the facet normal from 90°. ψ_2 is similarly calculated using the reflected ray. We require two additional quantities before calculating ρ_{s1}: the surface roughness of the facet, σ_h, and the wave number of the transmitter, $2\pi/\lambda$, where λ is the transmitted wavelength. Given these, ρ_{s1} is now

$$\rho_{s1} = e^{-2 \cdot \left(\frac{2\pi\sigma_h}{\lambda} \sin(\psi_1)\right)^2} \tag{3}$$

and similarly for ρ_{s2}, with ψ_2 in place of ψ_1 in Equation (3). Thus, Barton scales σ^0 by the factor

$$F_d^{\,2} = \sqrt{(1 - \rho_{s1}^2)\,(1 - \rho_{s1}^{\,2})} \tag{4}$$

Note that this term goes to zero as either ψ_1 or ψ_2 goes to zero.

Another multiplicative factor in the bistatic radar cross section is the Fresnel reflection coefficient, ρ_o. In the model, this quantity can be calculated using dielectric constants for a variety of terrains both wet and dry and for either horizontal or vertical polarization. The result for vertical polarization is

$$\rho_o = \frac{\varepsilon \sin\psi_1 - (\varepsilon - \cos^2\psi_1)^{1/2}}{\varepsilon \sin\psi_1 + (\varepsilon - \cos^2\psi_1)^{1/2}} \tag{5}$$

where ε is the complex dielectric constant and ψ_1 is the angle of incidence defined above. Finally, the bistatic scattering coefficient is multiplied by a vegetation (trees, bushes, etc.) dependent term ρ_v. This results finally in the quantity

$$\sigma = \sigma^0 \cdot F_d^{\,2} \, |\rho_o|^2 \rho_v^{\,2} \tag{6}$$

which is defined as the bistatic radar cross section.

Given the radar cross section, we can calculate the receiver sum voltage signal for a facet via the equation

$$\Delta_{sum} = \frac{\lambda}{R_1 \cdot R_2} \left[\frac{P_T \cdot A \, \sigma}{(4\pi)^3} \right]^{1/2} F_T \tag{7}$$

where

- λ = transmitted wavelength;
- R_1 = range from transmitter to facet center;
- R_2 = range from facet center to receiver;
- P_T = the transmitted power;
- A = the facet area;
- σ = the bistatic radar cross section;
- F_T = the transmitter gain factor.

The transmitter gain factor is the transmitter pattern gain in the direction of the facet. The calculation of these gains is discussed more fully in Section 3.

1.3 THE DIFFUSE DOPPLER MODEL

The program computes the diffuse contribution from each facet and adds it coherently to the receiver sum channel. For diffuse multipath, the assumption is that the voltage return from each facet has a random phase associated with it where the phases of all the facets at an instant in time are uniformly distributed over 0° to 360°. Statistically, this assumption causes the diffuse return to be distributed as a bivariate Gaussian. Thus, each Δ_{sum} is multiplied by a complex bivariate Gaussian with unit variance. The result is

$$\Delta_{sum} \frac{(N_1 + j\, N_2)}{\sqrt{2}} \tag{8}$$

where N_1 and N_2 are independent zero mean, unit variance Gaussian random variables and j is the square root of -1. The total diffuse voltage signal, D_T, is the sum over M facets of the above terms or

$$D_T = \sum_{i=1}^{M} \Delta_{sum} \frac{(N_1 + j\, N_2)}{\sqrt{2}} . \tag{9}$$

The calculations for the difference channels are very similar. Note that the Doppler dependence of D_T is buried in the above sum. The computer model is thus forced to break this sum down into separate Doppler parts.

The calculation of the Doppler shift itself is very straightforward since only the shift relative to the transmitter frequency is considered. Thus, the total shift is computed as the sum of the shift between the facet and the target and the facet and the receiver. Data storage considerations require that the program use discrete Doppler bins for the multipath. Each Δ_{sum} term is then added to the Doppler bin containing the frequency at which it was received. The Doppler bins used in this program are 100 Hz wide, and in the data tables delivered to MICOM the line of sight frequency is fixed as bin number 45 in a bin set spanning 6400 Hz. The resulting histogram provides an approximation to the Doppler frequency spectrum.

1.4 THE APPARENT DIRECTION

Specifying the apparent direction of the diffuse and specular multipath signals was an important requirement on this project. This requirement is based on the hardware configuration in the RFSS where only a limited number of signal sources can be active at one time. A single source, a triad of horns, was designated for providing the diffuse multipath at a single instant along the flight path, and another independent source was used to transmit the specular signal. The RFSS uses information from the lookup tables to determine the location of these sources. The apparent direction is defined to be the direction to the location from which the multipath signal appears to be coming with respect to the missile. The assumption is that illuminating from this location provides the same missile response as the actual diffuse and specular signal environment.

For the specular multipath, the apparent direction is found simply by computing the specular angle in the ground plane (assumed to be flat). The computation of the apparent direction for the diffuse signal is more complicated and is based upon a classical sum and difference tracker. One difficulty with this approach is that the apparent track error location can change with boresight direction; an omnidirectional antenna pattern was used to overcome this problem. The details of the derivation are given below.

The classical radar tracking problem consists of determining the elevation and azimuth angle errors, ϕ_ε and ϕ_α respectively, off the missile boresight. For the simplest case of a single point target, these angle errors identify the target's location with respect to the missile pointing direction. The assumption is made that the angle errors are proportional to the real part of the ratio of the voltage difference channel, D, to the voltage sum channel, S. Thus, the angle errors can be written as

$$\phi_\varepsilon = \text{Real } \{P_e \frac{D}{S}\} , \qquad (10)$$

$$\phi_\alpha = \text{Real } \{P_a \frac{D}{S}\} , \qquad (11)$$

where P_e and P_a are the constants of proportionality. The angle error is assumed to be zero when the missile is pointed directly at the target. The proportionality constants are computed by evaluating the D/S ratio for a small angle and a point target. For example, the elevation proportionality constant is computed as

$$P_e = \delta_\varepsilon \text{ Real } \{\frac{S}{D}\} \tag{12}$$

where δ_ε is a small elevation angle and the sum and difference signals correspond to the sum and difference patterns evaluated at the angle δ_ε. For the diffuse multipath problem, the Gaussian sum, f_S, and difference, f_D, patterns

$$f_S(\theta_e, \theta_a) = e^{-C(\theta_e^2 + \theta_a^2)} \tag{13}$$

$$f_D(\theta_e, \theta_a) = \begin{cases} \frac{d}{d\theta_e} f_S(\theta_e, \theta_a), & \text{elevation} \\ \frac{d}{d\theta_a} f_S(\theta_e, \theta_a), & \text{azimuth} \end{cases} \tag{14}$$

are assumed, where θ_e and θ_a are the elevation and azimuth angles off boresight. The constant, C, controls the beamwidth of the pattern and drops out of the equations later on. Using the Gaussian patterns, the proportionality constant for elevation becomes

$$P_e = \delta_\varepsilon \frac{e^{-C(\delta_\varepsilon^2 + \theta_a^2)}}{-2C\delta_\varepsilon\, e^{-C(\delta_\varepsilon^2 + \theta_a^2)}} = -\frac{1}{2C} \tag{15}$$

and the angle error for a point target is given by

$$\begin{aligned} \phi_\varepsilon &= P_e \frac{D}{S} \\ &= (-\frac{1}{2C}) \left[\frac{-2C\theta_e\, e^{-C(\theta_e^2 + \theta_a^2)}}{e^{-C(\theta_e^2 + \theta_a^2)}} \right] = \theta_e . \end{aligned} \tag{16}$$

The diffuse multipath case is complicated because the sum and difference signals are formed by contributions from many facets. Thus, the S and D in the Equations (10) and (11) are replaced by the total summations over all the facets. In particular, the elevation angle in Equation (16) becomes

$$\phi_\varepsilon = P_e \text{ Real} \left\{ \frac{\sum D_i}{\sum S_i} \right\} = \left(-\frac{1}{2C}\right) \text{Real} \left\{ \frac{\sum -2C\ \theta_{e_i}\ S_i}{\sum S_i} \right\}$$

$$= \text{Real} \left\{ \frac{\sum \theta_{e_i}\ S_i}{\sum S_i} \right\} \tag{17}$$

A similar result holds for the azimuth angle.

1.5 THE SPECULAR RETURN

The specular multipath model is not as complicated as the diffuse model. The terrain is treated as a single plane, rather than many facets. Thus, it is easy to calculate the specular point and the specular angle since only analytic geometry is necessary. Once the specular point is determined, the beacon equation is used along with the specular reflection coefficient to calculate the specular multipath return. This results in the equation

$$S_T = \frac{\lambda \cdot \sqrt{P_T} \cdot G_t\ e^{i\frac{2\pi}{\lambda}(R_1 + R_2 - R)}}{4\pi \cdot (R_1 + R_2)} \cdot \rho \tag{18}$$

where

λ = transmitted wavelength,
P_T = transmitted power,
G_T = transmitter voltage pattern factor,
R_1 = distance from transmitter to specular point,
R_2 = distance from specular point to receiver,
R = line of sight distance from receiver to transmitter,

and the specular reflection coefficient, ρ , is computed as

$$\rho = \rho_o \; \rho_v \cdot e^{-2 \left(\frac{2\pi}{\lambda} \sigma_h \sin\psi\right)^2} \tag{19}$$

where

ρ_o	=	Fresnel reflection coefficient,
ρ_v	=	vegetation factor,
λ	=	wavelength of the transmitter,
σ_h	=	the surface roughness of the terrain at the specular point,
ψ	=	the specular angle.

The apparent location for the specular multipath is assumed to be the specular point. However, this point will appear to wander according to the dimensions of the first Fresnel zone. In [2], the major and minor axes of the glistening surface are given. Briefly, this results in a length of $4 \cdot \beta_o$ if the specular angle, θ , is less than $2 \cdot \beta_o$ or a length of $2 \cdot \beta_o + \theta$ otherwise. The width of the surface is given by $2 \cdot \theta \cdot \beta_o$. Scaling these values by 1/e provides the standard deviations for the aimpoint wander. Note that since β_o was fixed at 0.2 in both scenarios, the statistics of the apparent direction will not appear to vary much between encounter scenarios.

In summary, the lookup table for the specular program includes

1. the receiver's altitude,
2. the line of sight speed,
3. the line of sight range,
4. the elevation angle of the receiver boresight relative to the line of sight,

5. the standard deviation of this angle,
6. the azimuth angle of the receiver boresight relative to the line of sight,
7. the standard deviation of the azimuth angle,
8. the magnitude of the received signal voltage,
9. the Doppler shift of the received signal due to the motion of transmitter and receiver with respect to the terrain.

SECTION 2

TERRAIN MODEL

The multipath Doppler model was exercised for two different terrains: White Sands Missile Range and Eglin Air Force Base. Digitized representations of these terrains were obtained from data tapes furnished by the government. For purposes of this program, the facets on the tapes were assumed to be square, although one terrain is in fact made up of slightly rectangular facets. The data tapes consist of elevation data approximately every 80 meters over a large rectangular grid. The data tapes do not describe terrain type, decorrelation distances, or surface roughness. Thus, surrounding data points were used to obtain an average surface tilt and to calculate the surface roughness of the given facet. Since the exact vegetation of the terrains was unknown, the White Sands terrain was modeled as sand scrub, and the Eglin terrain was assumed to be grassy. The limits of the computer implementation are such that the size of the terrain data base is restricted to a size smaller than that required in many of the scenarios. In such cases, the terrain was "rolled over," that is, the piece of available terrain was mirrored in each direction as necessary during the flight. The mirroring effect provided continuity in the terrain's surface roughness and altitude data.

Each terrain model consists of a rectangular grid of facets which are characterized by the following parameters: elevation of the facet center, rms surface roughness, tilt, and terrain type.

Surface roughness and tilt for each facet were computed using a weighted least squares plane-fitting algorithm. Given N digitized points (X_i, Y_i, Z_i), $i = 1, 2, 3, \ldots, N$, a plane may be fitted to these points. The plane model is given by

$$\hat{Z} = C_1 + C_2X + C_3Y \tag{20}$$

where

C_1 = Z-intercept,
C_2 = slope in the X-direction,
C_3 = slope in the Y-direction.

The Z-coordinate error at each point is given by

$$\varepsilon_i = Z_i - \hat{Z}_i = Z_i - (C_1 + C_2X_i + C_3Y_i) \ . \tag{21}$$

If the error at each point is weighted by a factor W_i, then the total squared error is

$$E^2 = \sum_{i=1}^{N} (W_i \varepsilon_i)^2 = \sum_{i=1}^{N} W_i^2 (Z_i - C_1 - C_2X_i - C_3Y_i)^2 \ . \tag{22}$$

The values for C_1, C_2, and C_3 which yield the minimum squared error may be found by taking partial derivatives with respect to the C's and setting them to zero.

After the coefficients C_1, C_2, and C_3 have been found, the unit normal to the least squares plane is found to be

$$\hat{n} = (-\frac{C_2}{L}, -\frac{C_3}{L}, \frac{1}{L}) \tag{23}$$

where

$$L = (C_2^2 + C_3^2 + 1)^{1/2} \ . \tag{24}$$

The unit normal describes the facet tilt. It is used to determine the angles of incidence and reflectance and to test for simple self-shadowing in the Doppler multipath model.

For the White Sands terrain, surface roughness on a facet was also calculated from the digitized terrain data. It was computed as the root mean square error

$$E_{rms} = \left[\frac{\sum_{i=1}^{N} (W_i \varepsilon_i)^2}{\sum_{i=1}^{N} W_i} \right]^{1/2} . \tag{25}$$

A lower limit of 1 cm roughness was assigned for any facets with computed E_{rms} values less than 1 cm. This was done to account for the cases where zero E_{rms} values were obtained due to the coarseness of the terrain digitization. Zero surface roughness would imply a perfectly smooth reflecting surface, and the terrain being modeled did not have such characteristics.

The Eglin terrain, while gently sloping, does not exhibit large surface roughness. Rather than use the computed E_{rms} values to represent the facet roughness, the terrain model was forced to be smooth by using a constant 1 cm surface roughness for the Eglin terrain.

Terrain type is a qualitative switch in the multipath model which determines the selection of the vegetation factor and the dielectric constant. For White Sands the terrain type was assumed to be dry sand. This characterization led to the selection of a complex dielectric constant of

$$\varepsilon = 2.4 + j\,0.1 \tag{26}$$

obtained from Cihlar and Ulaby [7] with no vegetation attenuation ($\rho_v = 1$) . The Eglin terrain was described as grassy with a dielectric constant of

$$\varepsilon = 2.0 + j\,0.0 \tag{27}$$

with again no vegetation attenuation ($\rho_v = 1$) .

SECTION 3

ANTENNA PATTERNS

3.1 INTRODUCTION

Data were furnished to Georgia Tech for two different transmitters. Each transmitter was implemented separately in the bistatic Doppler multipath model. The nature of the data received and the methods of implementation are discussed below.

3.2 MEASUREMENT OF AZIMUTH AND ELEVATION

Figure 2 shows the scheme used for measuring angles. This particular scheme is referred to as azimuth over elevation because the azimuth angle is measured over the elevation plane. We shall use the abbreviation AZ/EL. First the elevation angle is determined by computing the orthogonal projection $\vec{F}_p$ of $\vec{F}$ onto the plane containing $\hat{z}$ and $\vec{L}$ and then taking the dot product of $\vec{L}$ with $\vec{F}_p$. Similarly, the azimuth angle is found by taking the dot product of $\vec{F}_p$ with $\vec{F}$. This method of determining azimuth and elevation provides answers which differ in some cases from those obtained by an alternative method. In the alternative method, elevation over azimuth (EL/AZ), the azimuth angle is determined first.

As an example of the measurement scheme, let us examine the elevation angle generated. Let $\vec{F} = (F_x, F_y, F_z)$ and $\vec{L} = (L_x, L_y, L_z)$. If

$$\vec{G} = \vec{F} - \frac{\vec{F} \cdot (\vec{L} \times \hat{z})}{|\vec{L} \times \hat{z}|^2} \quad (\vec{L} \times \hat{z}) \text{ , then} \tag{28}$$

$$\cos EL = \vec{G} \cdot \vec{L} \ / \ (|\vec{G}| \ . \ |\vec{L}|) \ . \tag{29}$$

Notice that $\vec{L} \times \hat{z} = (+L_y, -L_x, 0)$ so that

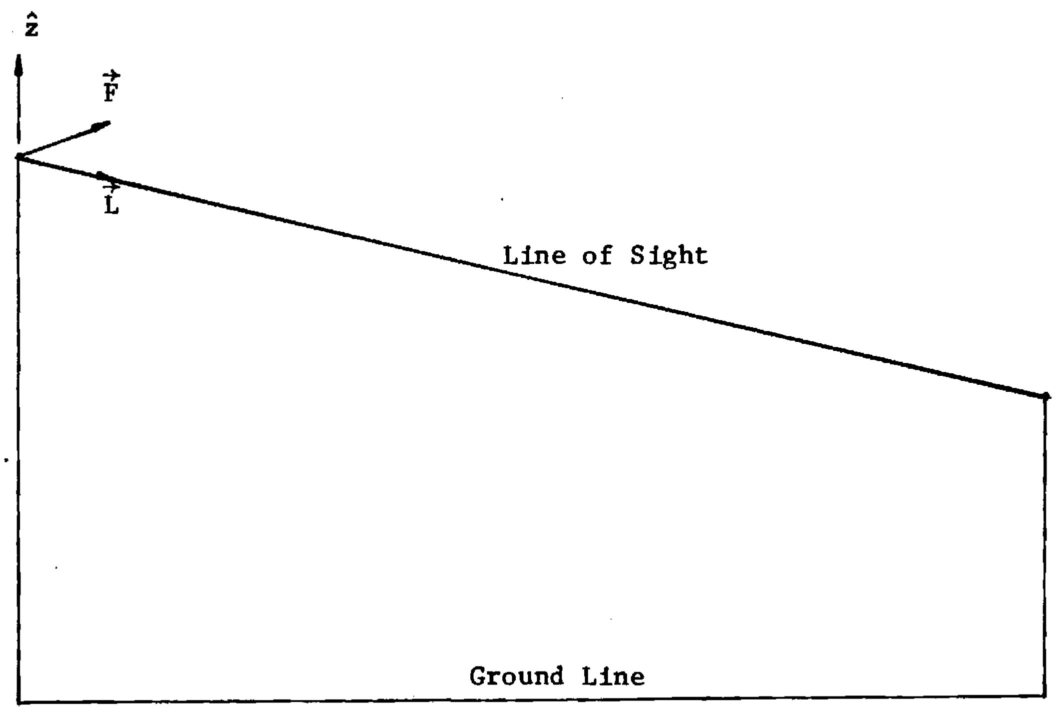

Figure 2. Illustration of the geometry used in the azimuth over elevation angle calculations.

$$\vec{G} = \vec{F} - \frac{F_x L_y - F_y L_x}{L_x^2 + L_y^2} (+L_y, -L_x, 0) \quad \text{and} \tag{30}$$

$$|\vec{G}| = \left[\frac{(F_x L_y - F_y L_x)}{(L_x^2 + L_y^2)} + F_z^2 \right]^{1/2} . \tag{31}$$

From these definitions, the AZ/EL result is

$$EL = \cos^{-1} [(\vec{F} \cdot \vec{L}) / (|\vec{G}| \cdot |\vec{L}|)] . \tag{32}$$

3.3 CONTRACTOR EAST DATA

Contractor EAST supplied MICOM with antenna measurement data on April 22, 1982. The data of interest were recorded at a frequency referred to as "H" for high. Both azimuth and elevation cuts were measured. The azimuth cuts were measured at elevation angles of 1°, 14°, 29°, and 44° off the boresight; the elevation cuts were measured at azimuth angles of 0°, 30°, and 60°. These antenna cuts were digitized using a bitpad and a digitizing program on the ECLIPSE S130 computer. Figure 3 illustrates the resulting digitized data. Since these antenna cuts were measured as great circle cuts, a series of transformations had to be applied to convert the angles measured during the running of the multipath program to great circle angles.

The transformations which were applied to this data are as follows:

$$\begin{aligned} AEEL &= \sin^{-1} (\cos\varepsilon \sin EL - \sin\varepsilon \cos AZ \cos EL); \\ AEAZ &= \tan^{-1} (\sin AZ \cos EL / (\cos\varepsilon \cos AZ \cos EL + \sin\varepsilon \sin EL)); \end{aligned} \tag{33}$$

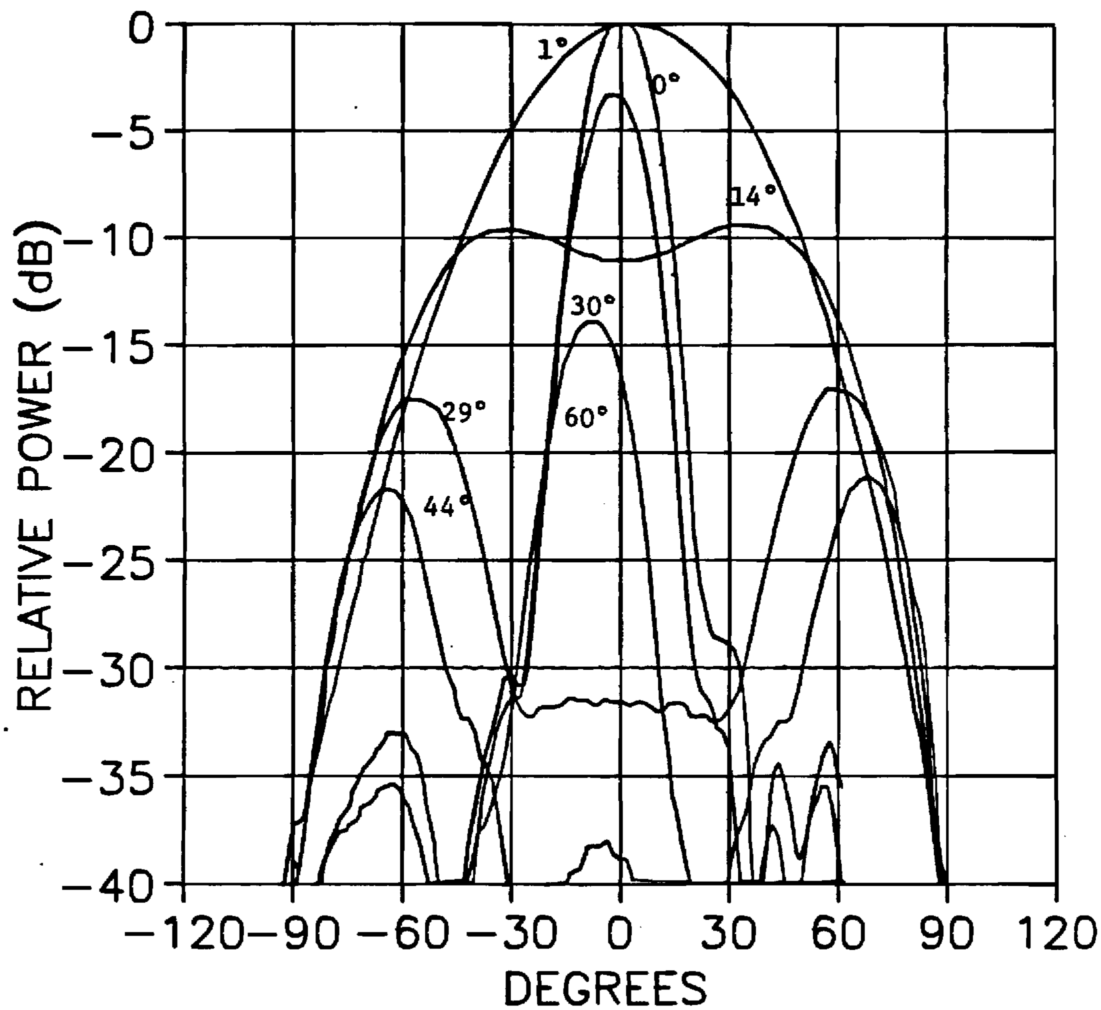

Figure 3. Display of both azimuth and elevation cut antenna data for Contractor EAST.

$$AAAZ = \sin^{-1} (\sin AEAZ \cos AEEL);$$
$$AAEL = \tan^{-1} (\tan AEEL/\cos AEAZ); \quad (34)$$

where:

- ε = the depression angle of the boresight off horizontal;
- EL = the elevation angle of the direction of interest relative to the boresight as computed in the multipath model;
- AZ = the azimuth angle of the direction of interest relative to the boresight as computed in the multipth model.

For this program ε was set either at -29° or -25° depending on whether the transmitter was assumed to be flying level or pitched up at 4°. The pattern peak gain was 0 dB and the assumed gain was 13.5 dB so 13.5 was added to each digitized data point.

3.4 CONTRACTOR WEST DATA

Contractor WEST supplied MICOM with antenna measurement data on April 22, 1982. The data of interest were recorded at a frequency referred to as F6. The data which were digitized were azimuth sweeps for varying elevation angles. The elevation angles ran from +10° above horizontal to -100°, in increments of 10°, except for an additional cut at -45°. These measurements were also great circle cuts; after the elevation and azimuth angles were determined, they were transformed by the relations

$$AAAZ = \sin^{-1} (\sin AZ \cos EL); \quad (35)$$

$$AAEL = \tan^{-1} (\tan EL/\cos AZ); \quad (36)$$

where AZ and EL are defined as the azimuth and elevation angles of the desired direction relative to the transmitter's boresight. In those cases where the vehicle was run pitched up at 4°, the program was modified so that the elevation cuts ran from 6° to -104°. Figure 4 displays the digitized data. The pattern peak gain was -4 dB and assumed gain was 15.4 dB, so 19.4 dB was added to each digitized data point.

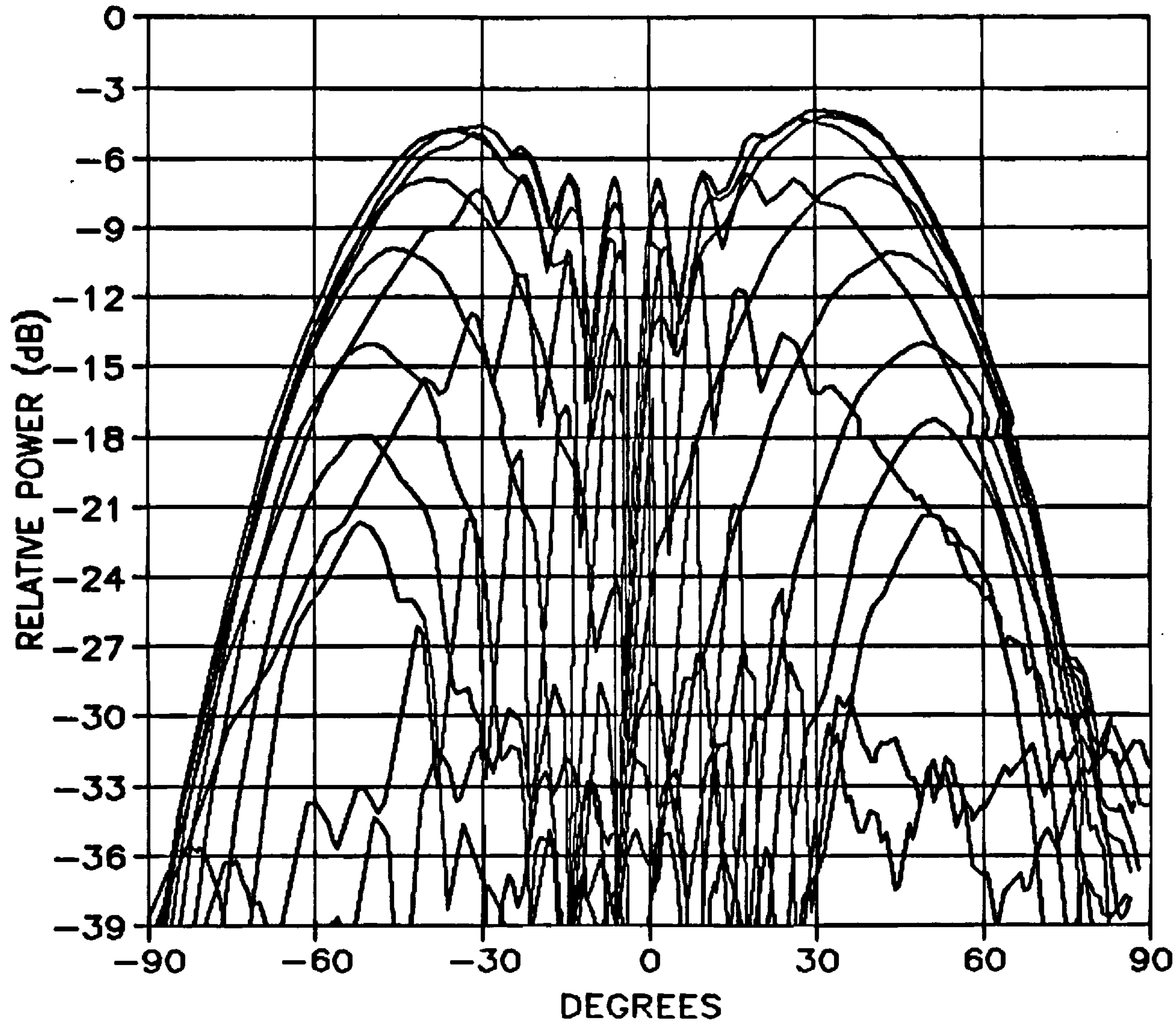

Figure 4. Display of azimuth antenna cut data for Contractor WEST.

SECTION 4

SIMULATED FLIGHT SCENARIOS

Georgia Tech produced Doppler multipath tables for a variety of flight scenarios used in the RFSS facility. The target was constrained to constant speed, straight and level flight at 300 foot and 600 foot altitudes. There were eight down range - cross range initial launch conditions. The down range - cross range pairs consisted of (8,0), (8,5), (16,0), (16,5), (16,10), (24,0), (24,5), and (24,10) kilometers as illustrated in Figure 5.

Five missile flight paths were generated for each of the sixteen encounter geometries by a MICOM supplied program. The objective was to produce flight conditions of sufficient variety to ensure reasonable interpolation within the multipath Doppler table during the RFSS simulation. The five different flight paths correspond to nominal "lock on" times of 1.3, 3, 5, 7, and 10 seconds. The flight paths were further manipulated to prevent intersections within a set of five paths. Intersections would severely complicate the interpolation scheme used during the RFSS simulation. The final set of five flight paths produced two paths ending above the target, two paths ending below the target, and the middle path intercepting the target.

Figures 6 through 8 illustrate the flight paths for the eight different launch geometries at the 300 foot target altitude. The units on the axes are kilometers and the tic marks on the curves represent ninety second intervals.

The final set of data delivered on this project consists of diffuse and specular Doppler multipath tables for each of the sixteen encounter geometries over both terrains for two different targets (128 tables in all). Each table contains the results of the diffuse (or specular) multipath model for every half second during the flight. During the RFSS simulation, the table is accessed with input values from the RFSS, and the Doppler multipath signal and apparent direction are obtained by interpolation. The input variables are closing speed (between

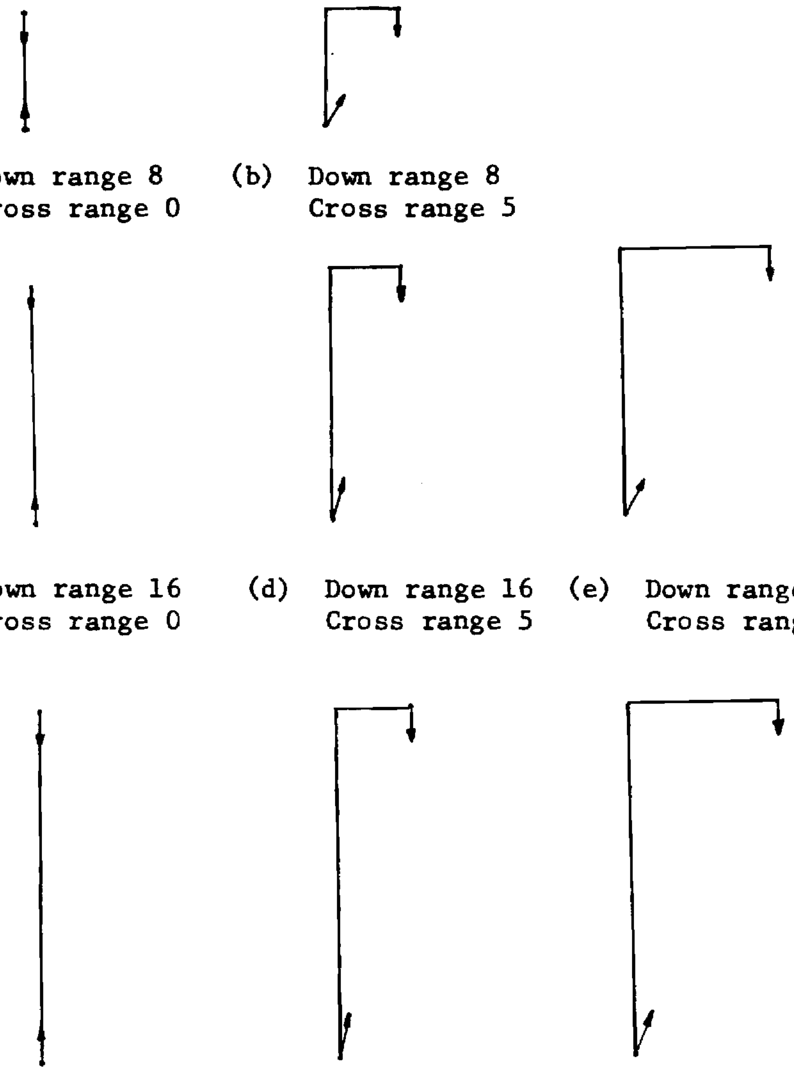

(a) Down range 8
Cross range 0

(b) Down range 8
Cross range 5

(c) Down range 16
Cross range 0

(d) Down range 16
Cross range 5

(e) Down range 16
Cross range 10

(f) Down range 24
Cross range 0

(g) Down range 24
Cross range 5

(h) Down range 24
Cross range 10

Figure 5. Illustration of the down and cross range launch conditions.

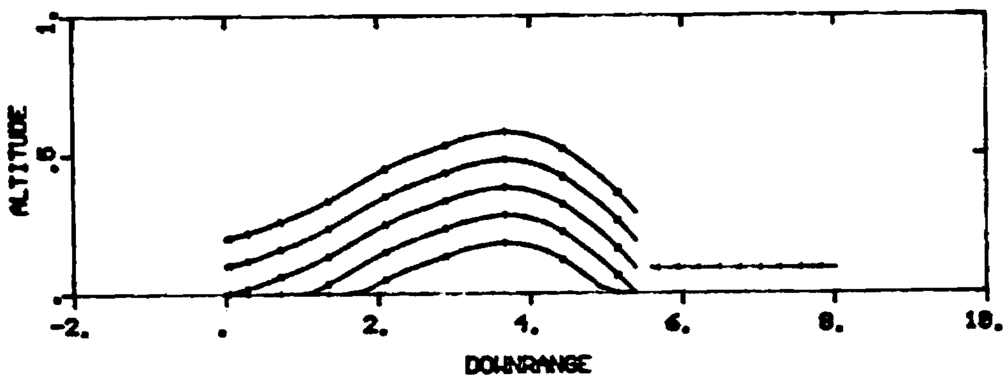

6a. 0 kilometer cross range

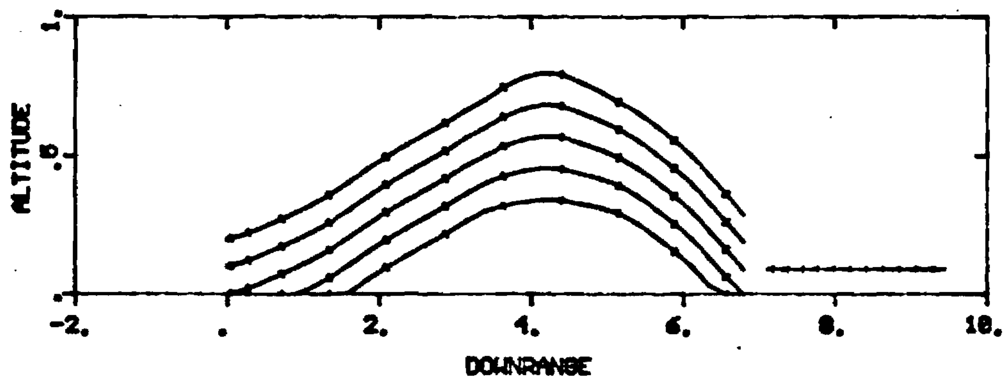

6b. 5 kilometer cross range

Figure 6. Samples of the model flight paths for 8 kilometer down ranges and 300 foot target altitude.

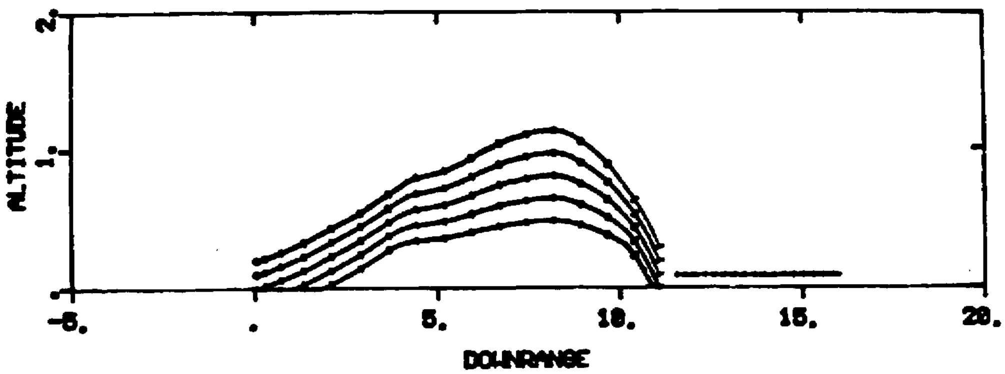

7a. 0 kilometer cross range

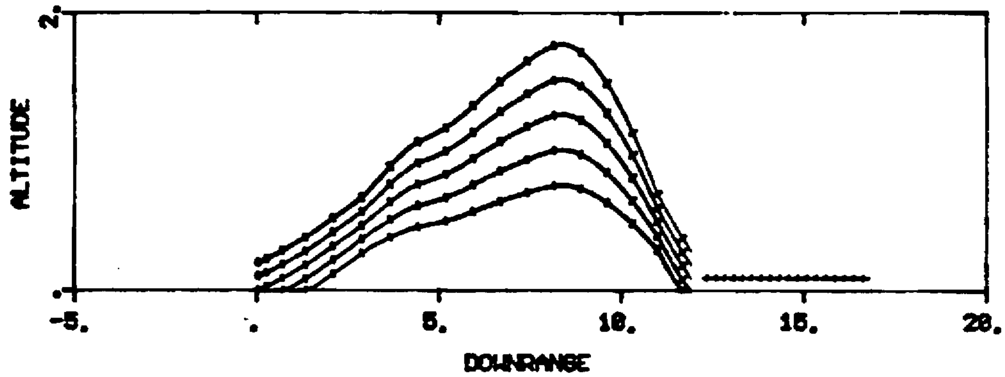

7b. 5 kilometer cross range

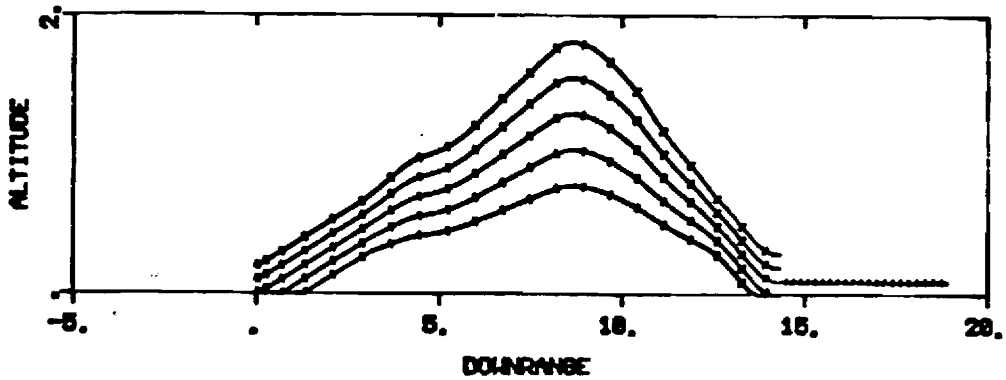

7c. 10 kilometer cross range

Figure 7. Samples of the model flight paths for 16 kilometer down ranges and 300 foot target altitude.

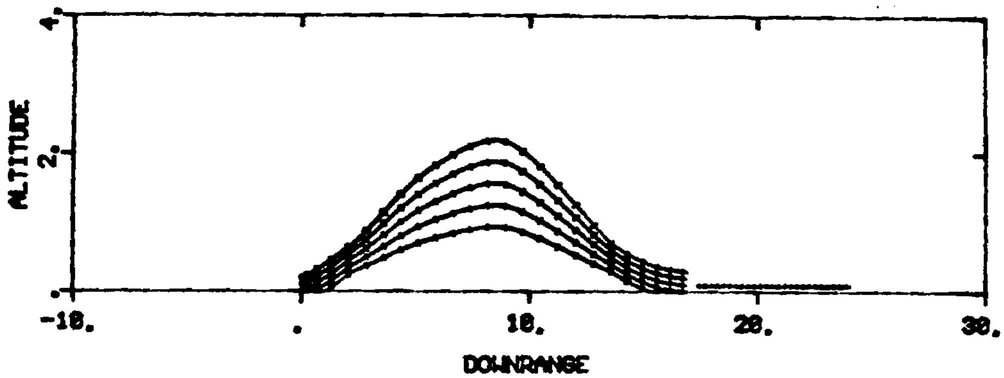

8a. 0 kilometer cross range

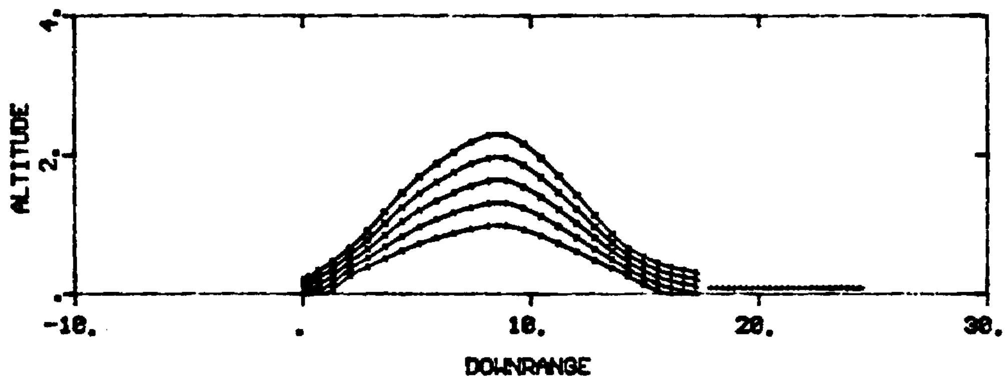

8b. 5 kilometer cross range

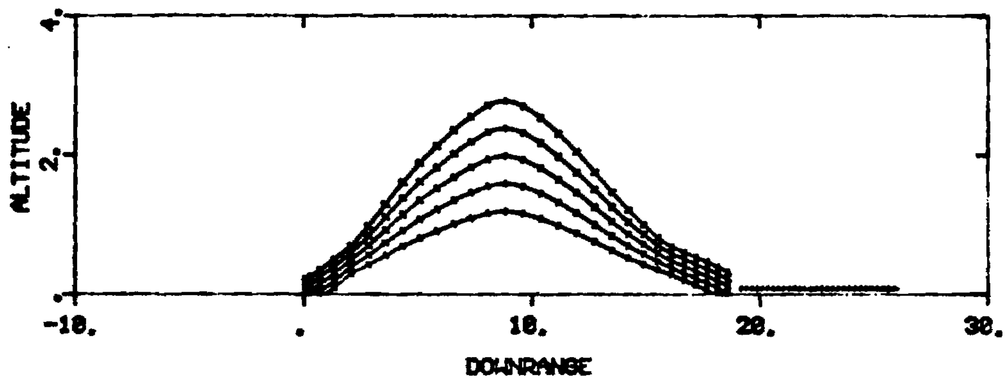

8c. 10 kilometer cross range

Figure 8. Samples of the model flight paths for 24 kilometer down ranges and 300 foot target altitude.

the missile and target), missile altitude, and the range between the target and the missile. Altitude and range are listed in meters, and the closing speed is given in meters per second. The apparent direction of the diffuse signal is described in the table by the mean azimuth and elevation angles and their respective standard deviations. The multipath signal is presented as a Doppler spectrum of expected power levels. The spectrum is composed of sixty-four 100 Hz bins. Bin 45 corresponds to the line of sight Doppler bin. The Doppler shift for this bin is also given for each point in time along each flight path in the table.

During the RFSS simulation, the tabulated spectrum can be shifted according to the difference between the real-time simulation and the tabulated closing speeds. The power levels on the signal are also adjusted corresponding to the actual transmitted powers and antenna gains being used.

SECTION 5

SUMMARY AND CONCLUSIONS

Over 128 separate bistatic multipath Doppler scenarios were provided to MICOM from a model which was developed, implemented, and tested in less than three months. Time constraints made some mistakes almost inevitable, but a close working relationship with Boeing and MICOM helped head off many potential problems. The data provided included:

1. Relative positions of receiver and transmitter as a function of time.
2. Apparent locations in azimuth and elevation for both the diffuse and specular multipath.
3. Standard deviations to further describe the above locations.
4. Doppler information for the significant frequencies surrounding the line of sight Doppler frequency.
5. The total multipath specular and diffuse voltage signals as a function of time.

The bistatic Doppler multipath model developed by Georgia Tech demonstrated the ability, through software, to quickly modify and update multipath contributions to a broad range of scenarios. For example, intercept flight paths can be quickly altered, and new data can be obtained much faster than in a test environment totally dependent on hardware.

Quick turn-around is also available for changing such items as antenna patterns, terrains, transmitted powers, gains, etc. On the other hand, the data obtained from software models can be no better than the inputs to such models, and several areas in the Georgia Tech model could be improved.

One of the weak areas in the model is the terrain data base. The data which were made available were not sufficient for an accurate model of the desired landscapes. In particular, the calculation of surface roughness and facet tilts had to be crudely approximated, given the large distances between data points.

A thorough review of the angle measuring schemes used in the multipath model could prove very useful for avoiding problems in the future with the modeling of various antenna systems. In particular, the AZ/EL versus EL/AZ question needs to be investigated in greater detail with regard to the measurement of the antenna patterns. This is an important task which is necessary to avoid errors in using measured antenna patterns.

The theory inherent in the multipath program has been thoroughly reviewed in the course of preparing this report and no errors in the implementation of the theory were discerned. However, the program shows evidence of hasty patching and programming compromises. Further efforts in multipath analysis should be accompanied by program restructuring.

Numerous possible improvements of the model are worthy of consideration, i.e.,

1. Integrate the flight path scenario generator with the track error generator multipath model.
2. Implement the other factors in the encounter scenario such as clutter and plume attenuation.
3. Georgia Tech has the capability to generate a graphical picture of what the receiver "sees," such as the specular flashes from the terrain, the multipath isodops, the intensity of the diffuse multipath from each terrain facet, etc. This would be an ex+remely desirable tool from an interactive analysis standpoint and since this information is already calculated, the display of it would be a straightforward process.
4. The theory used in the model is believed to be the best available. The fact that extensive measurement data will shortly be available for comparison with the model data provides a unique opportunity to further refine the existing model. In particular, low altitude dependencies and

apparent directions are both areas open to considerable refinement.

References

1. David K. Barton, "Low-Angle Radar Tracking," Proceedings of the IEEE, Vol. 62, No. 6, June 1974, pp. 687 -704.

2. David K. Barton, "Low-Altitude Tracking Over Rough Surfaces I: Theoretical Predictions," EASCON-79 Record.

3. P. Beckmann and A. Spizzichino, The Scattering of Electromagnetic Waves from Rough Surfaces, Pergammon, New York, 1963.

4. S. P. Zehner, M. T. Tuley, "Development and Validation of Multipath and Clutter Models for TAC ZINGER in Low Altitude Scenarios," Final Report on Contract F49620-79-C-0121, Georgia Institute of Technology, Engineering Experiment Station, March 1979.

5. S. P. Stuk, "TAC ZINGER Clutter and Multipath Models for Track-While-Scan Systems," Software Documentation on Contract No. F49620-79-C-0222, Georgia Institute of Technology, Engineering Experiment Station, October 1980.

6. R. L. Cook and K. E. Torrance, "A Reflectance Model for Computer Graphics," Computer Graphics, Volume 15, Number 3, August 1981, pp. 307-316.

7. J. Cihlar and F. T. Ulaby, "Dielectric Properties of Soils as a Function of Moisture Content," The University of Kansas Center for Research, Inc, RSL Technical Report 177-47, November 1974.